Transport of smoke from Canadian forest fires to the surface near Washington, D.C.: Injection height, entrainment, and optical properties

P. R. Colarco,[1] M. R. Schoeberl,[2] B. G. Doddridge,[3] L. T. Marufu,[3] O. Torres,[4] and E. J. Welton[2]

Received 14 October 2003; revised 4 January 2004; accepted 13 January 2004; published 19 March 2004.

[1] Smoke and pollutants from Canadian forest fires are sometimes transported over the United States at low altitudes behind advancing cold fronts. An unusual event occurred in July 2002 in which smoke from fires in Quebec was observed by satellite, lidar, and aircraft to arrive over the Washington, D.C., area at high altitudes. This elevated smoke plume subsequently mixed to the surface as it was entrained into the turbulent planetary boundary layer and had adverse effects on the surface air quality over the region. Trajectory and three-dimensional model calculations confirmed the origin of the smoke, its transport at high altitudes, and the mechanism for bringing the pollutants to the surface. Additionally, the modeled smoke optical properties agreed well with aircraft and remote sensing observations provided the smoke particles were allowed to age by coagulation in the model. These results have important implications for the long-range transport of pollutants and their subsequent entrainment to the surface, as well as the evolving optical properties of smoke from boreal forest fires. *INDEX TERMS:* 0305 Atmospheric Composition and Structure: Aerosols and particles (0345, 4801); 0345 Atmospheric Composition and Structure: Pollution—urban and regional (0305); 0360 Atmospheric Composition and Structure: Transmission and scattering of radiation; 0365 Atmospheric Composition and Structure: Troposphere—composition and chemistry; *KEYWORDS:* smoke aerosols, optical properties, entrainment

Citation: Colarco, P. R., M. R. Schoeberl, B. G. Doddridge, L. T. Marufu, O. Torres, and E. J. Welton (2004), Transport of smoke from Canadian forest fires to the surface near Washington, D.C.: Injection height, entrainment, and optical properties, *J. Geophys. Res.*, *109*, D06203, doi:10.1029/2003JD004248.

1. Introduction

[2] Ozone (O_3) and aerosols transported over long distances can affect air quality at local, regional, and even intercontinental scales. For example, the air over the Mediterranean contains a complicated mix of pollutants transported from Asia, North America, and Europe [*Lelieveld et al.*, 2002]. Saharan dust transported to the United States in the summertime occasionally contributes enough to surface level aerosol concentrations to put portions of Florida out of compliance with U.S. Environmental Protection Agency (EPA) standards for fine particulate matter [*Prospero et al.*, 2001]. Of particular interest in this paper is the transport of pollutants associated with emissions from boreal forest fires. Extensive areas in the boreal forests burn every year with significant interannual variability [*Lavoué et al.*, 2000]. These fires produce large amounts of aerosol and trace gas species, including carbon monoxide (CO) and nitrogen oxides (NO_x), important precursors to the photochemical production of tropospheric ozone [*Goode et al.*, 2000]. For example, enhanced surface level concentrations of CO observed during summer 1995 in the eastern and southeastern United States were attributed to pollutants produced and transported in the plumes from large Canadian forest fires [*Wotawa and Trainer*, 2000]. Transatlantic transport of boreal fire emissions can also be important, with several studies focusing on aspects of an event in August 1998 in which pollutants from fires burning in the Canadian Northwest Territories were transported over the Atlantic and into western Europe. *Forster et al.* [2001] attributed observations of enhanced surface level concentrations of CO at Mace Head, Ireland, and aerosol layers between 3 and 6 km altitude over Germany to this fire event. *Spichtinger et al.* [2001] used satellite imagery to track the transport of a NO_x plume associated with the same burning event. *Fiebig et al.* [2002, 2003] discuss the evolution of the smoke aerosol optical and microphysical properties for the plume observed in this event.

[3] Here we discuss a case of smoke from Canadian forest fires transported in an initially midtropospheric altitude plume that was observed at the National Aeronautics and Space Administration (NASA) Goddard Space Flight Center (GSFC, 39.02°N, 76.86°W, near

[1]Earth System Science Interdisciplinary Center, University of Maryland, College Park, Maryland, USA.
[2]NASA Goddard Space Flight Center, Greenbelt, Maryland, USA.
[3]Department of Meteorology, University of Maryland, College Park, Maryland, USA.
[4]Joint Center for Earth Systems Technology, University of Maryland Baltimore County, Baltimore, Maryland, USA.

0148-0227/04/2003JD004248$09.00

Washington, D.C.) and was subsequently mixed to the surface when it was intercepted by the turbulent planetary boundary layer (PBL). Over the period 5–9 July 2002, lightning initiated multiple fires in central Quebec which burned about 250,000 ha (1 ha = 10^4 m^2) of boreal forest (see Canadian fire statistics at http://www.nrcan.gc.ca/cfs-scf/science/prodserv/firereport/archives/july1002_e.html). An upper level low-pressure system over the Canadian Maritime Provinces coupled with a high-pressure ridge to the west channeled the smoke and pollutants from the fires about 1000 km southward into the eastern United States. These plumes were clearly visible in satellite imagery (Figure 1a), and aerosol optical thickness (AOT) retrievals from the Earth-Probe Total Ozone Mapping Spectrometer (EP-TOMS) satellite instrument [*Torres et al.*, 2002] showed that the plumes were optically thick (Figure 1b). During the passage of the plumes the U.S. east coast experienced some of the worst air quality days of the summer.

[4] In this paper we present an analysis of this event using remotely sensed and in situ data in combination with back trajectory calculations and simulations with a three-dimensional aerosol microphysical and transport model. In Section 2 we discuss the evolution of the plume vertical profile during transport in the context of lidar and aircraft observations and back trajectory calculations, and confirm its initially high altitude over the source region. In Section 3 we present our aerosol model and discuss the transport of the smoke plume from an elevated layer to the surface. In Section 4 we discuss the smoke aerosol optical properties and compare retrievals from remote sensing instruments with calculations from our simulations. We discuss our results and suggest future directions for this work in Section 5. Descriptions of our aerosol model and our approach to calculating aerosol optical properties is presented in Appendix A.

2. Evolution of the Plume Vertical Structure

[5] The NASA Micro-Pulse Lidar NETwork (MPLNET) [*Welton et al.*, 2001] operates a lidar at GSFC, colocated with a sun/sky photometer in the Aerosol Robotic NETwork (AERONET) [*Holben et al.*, 1998]. Figure 2 shows the MPLNET normalized relative backscatter ratio [*Campbell et al.*, 2002] measured by the lidar over the period 6–9 July 2002. These measurements show a smoke layer between 2 and 3 km arriving at GSFC late on 6 July. On 7 July the smoke plume rapidly mixed to the surface after about 12:00 UTC. Note that the lidar signal is completely attenuated above about 2 km altitude by the thick smoke plume at around 00:00 UTC on 7 July and also above about 1 km after the plume has been mixed to the surface later on 7 July. Because of this we do not have any information on the maximum altitude of the smoke layer at these times. On 8 July the lidar signal shows that some remnants of the smoke plume persist above the PBL at about 2–3 km altitude. The lidar was turned off after about 12:00 UTC on 8 July and did not make any further observations of this event. Also shown in Figure 2 is the PBL height at GSFC from the National Center for Atmospheric Research (NCAR) Model for Atmospheric Transport and Chemistry (MATCH) [*Rasch et al.*, 1997]. The peak height of the MATCH PBL is as high as the top of the lidar signal return at 18:00 UTC on 7 July, and the subsequent collapse of the model's PBL later in the day is consistent with the observed plume descent and mixing to the surface.

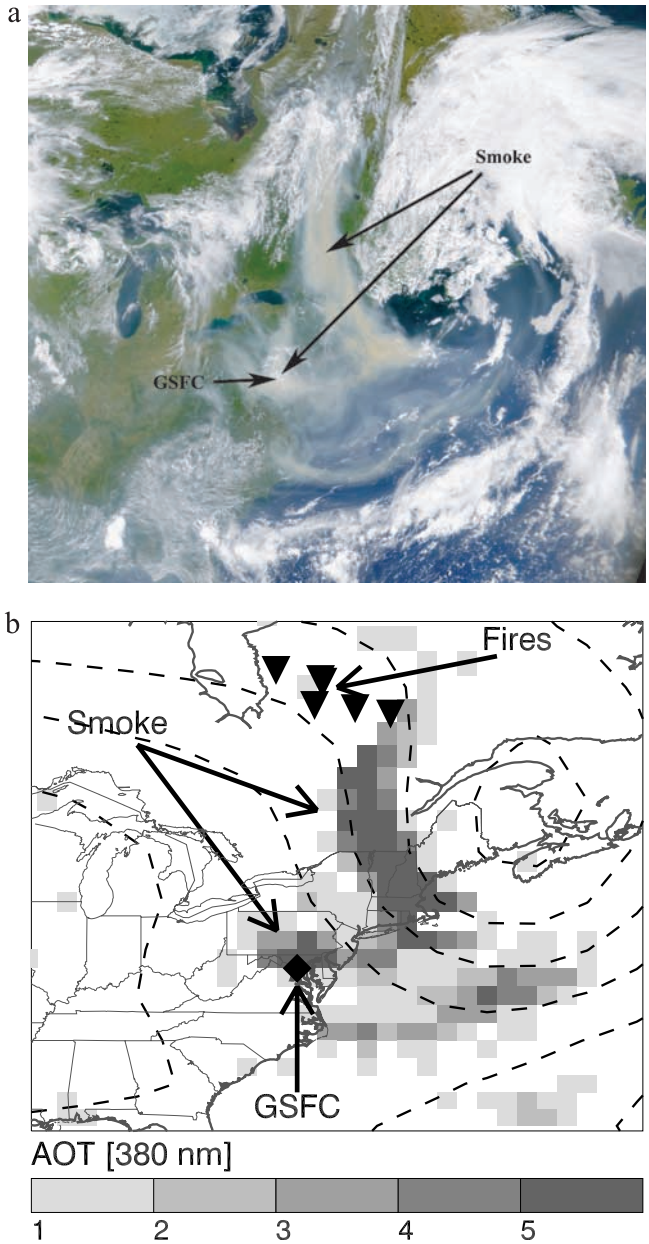

Figure 1. (a) Visible imagery from SeaWiFS space-based sensor on 7 July 2002 of the smoke plumes transiting from Quebec over the northeastern United States. (b) EP-TOMS-retrieved aerosol optical thickness (AOT) at 380 nm for 7 July 2002. Also shown are fire locations identified from GOES-8 imagery (triangles). We have also overplotted geopotential height contours on the 700 hPa surface from the NCEP/NCAR reanalyses (dashed lines). The minimum contour is at 3060 m altitude over Nova Scotia, and the contours increase in altitude from there in 40 m increments.

[6] Kinematic back trajectories were run with the NASA GSFC trajectory model [*Schoeberl and Sparling*, 1995] using National Center for Environmental Prediction

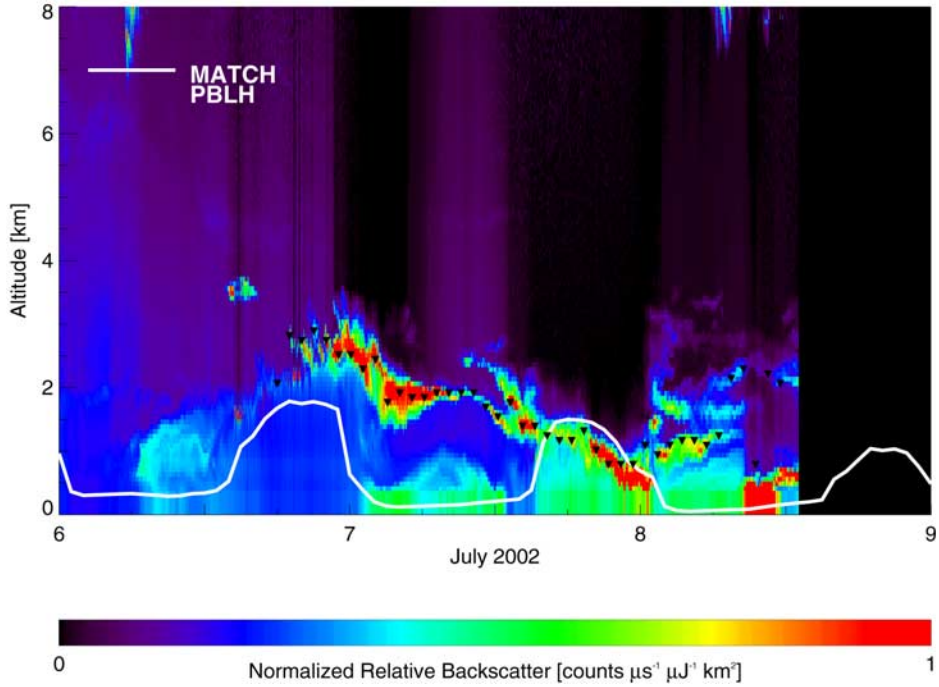

Figure 2. Vertical profile of aerosol backscatter observed at GSFC by MPLNET. The white line is the MATCH PBL height. The triangles indicate the initial altitude used in the back trajectories shown in Figure 3. Note that MPLNET did not collect data after about 12:00 UTC on 8 July 2002 until late on 9 July 2002.

(NCEP)/NCAR reanalyses [*Kalnay et al.*, 1996] to drive the calculations. Two-day back trajectories were initialized at 1.5, 3, and 4.5 km altitude over GSFC every hour between 18:00 UTC 6 July and 12:00 UTC 8 July. These calculations indicate that the air parcels over GSFC during this period (a) had their origins 1–2 days earlier over the regions being burned in Canada and (b) had descended from higher altitudes in the midtroposphere as they transited from Canada toward GSFC, consistent with the meteorological situation illustrated in Figure 1.

[7] Figure 3 shows 2-day back trajectories initialized every hour over this same time period at GSFC, where the initial altitude at GSFC is the altitude of the peak backscatter ratio observed by MPLNET. We determine the plume altitude by considering only backscatter at altitudes above 0.75 km so that we are not biased by low-altitude anthropogenic pollutants. The times the fires were actively burning in Quebec were determined from GOES-8 geostationary satellite imagery [*Prins and Menzel*, 1992] and are indicated by the grey hatched bars in Figure 3. For each trajectory we show the time and the altitude it crosses southward of 51°N, roughly the southern edge of the fire region identified from the GOES-8 imagery. For almost all of the trajectories this point occurred during or shortly after the period when the fires were active on 5 July. The trajectories were between 2 and 6 km altitude over the fire region and descended during transport. Trajectories at higher altitudes over the fire region were transported to GSFC more rapidly than those that were at lower altitudes. At times when the lidar signal is attenuated above low-altitude smoke it is possible that higher-altitude aerosol actually present would indicate somewhat higher trajectories crossing out of the fire region.

[8] The MPLNET data show elevated aerosol layers persisting on 8 July, with peaks in the backscatter intensity at around 2–3 km altitude. Portions of these aerosol layers in the GSFC/Washington, D.C., area were profiled several times on this day with the University Research Foundation-Advanced Development Laboratory's twin engine Piper

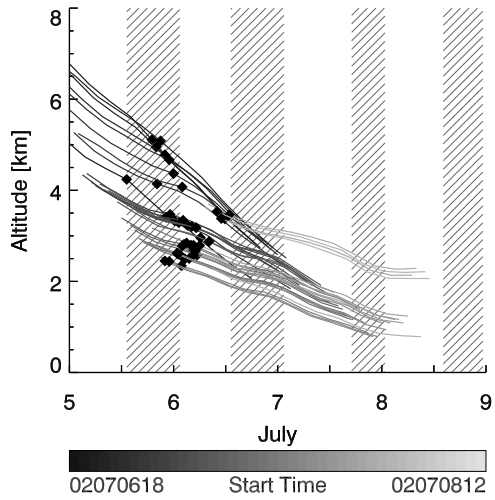

Figure 3. Two-day back trajectories from GSFC at the altitude of the observed peak MPLNET backscatter. The shading of the line indicates the start time of the trajectory, as does the right-hand endpoint x coordinate of the trajectory line. The grey hatched bars show the times the fires were active in Quebec as inferred from GOES-8 imagery. The diamonds on each trajectory show the time at which the trajectory passed south of 51°N.

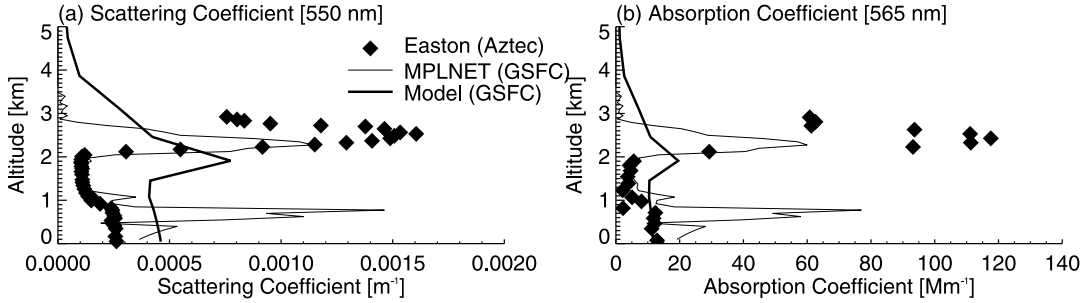

Figure 4. Observed and modeled aerosol (a) scattering and (b) absorption profiles at Easton on 8 July 2002. Shown are the Aztec profiles (diamonds) and the model profiles at 20:00 UTC (thick lines). Also shown are the MPLNET measurements of scattering and extinction at GSFC at 11:30 UTC (thin line).

Aztec-F PA-23-250 research aircraft. The Aztec was outfitted with an atmospheric research package run by the University of Maryland [*Taubman et al.*, 2004]. Particle scattering measurements were made with a three-channel integrating nephelometer operating at 450, 550, and 700 nm. Aerosol absorption was measured with a particle/soot absorption photometer operating at 565 nm. Additional measurements made include particle number concentrations and CO and O_3 mixing ratios. Five vertical profiles were made from near the surface to the aircraft's operational ceiling at 3 km, four of which were dominantly influenced by plume material from the Canadian fires. A fifth profile was flown to the west of the main smoke plume and was more strongly influenced by anthropogenic pollutants in the PBL. The profiles spanned a region about 200 km east-west over Maryland and northern Virginia and occurred over a period of about 8 hours. There is some variability in the smoke aerosol properties owing to the time and space variations in the plume. For the four profiles which showed evidence of the smoke plume, it was always at about 2–3 km altitude and had distinctly different scattering and absorption properties from the aerosols in the PBL. Back trajectories calculated from this 2–3 km range show that for each profile the air passed over the fire regions during the burning on 5 July at about 4 km. Finally, for all of these profiles the enhanced aerosol scattering and absorption occurs at the same altitude as the enhanced particle number concentrations and CO and O_3 mixing ratios.

[9] Figure 4 shows the narrow layer of aerosol scattering and absorption observed in the smoke plume on the Aztec profile flown above Easton, MD (38.80°N, 76.06°W, about 70 km E of GSFC, profile flown between 19:45 and 20:12 UTC). Also shown are the scattering and absorption profiles from the MPLNET data at GSFC at 11:35 UTC 8 July (determined from the retrieved extinction profile and the colocated AERONET single-scatter albedo retrieval discussed below), which show a peak in the 2–3 km altitude range. The MPLNET data also show a strong scattering and absorption peak below 1 km. Because of the high extinction-to-backscatter ratio determined for the MPLNET lidar profile it is likely that this low-altitude peak is due to remnants from the smoke plume intercepted at the surface on 7 July. This low-altitude peak is presumably not seen by the aircraft because of the temporal and spatial variability existing in the plume.

[10] In summary, the MPLNET data show the arrival of an elevated aerosol layer on 6 July, which was subsequently mixed to the surface on 7 July. Remnants of the elevated aerosol layers persisted on 8 July and were profiled both with MPLNET and a light aircraft. Back trajectory calculations support a hypothesis that the air parcels arriving over GSFC during this period had their origins at 2–6 km altitude over fires burning in Quebec 1–2 days earlier and that the air had descended during its transit.

3. Mixing of the Smoke Plume to the Surface

[11] On 6 and 7 July surface ozone levels were low over most of the northeastern United States (see surface ozone data from the Environmental Protection Agency at http://www.epa.gov/airnow/2002/). The pollutants from the Canadian fires had not yet been transported to the surface. Figure 5a shows, however, that on 8 July there were very high surface mixing ratios of ozone (mixing ratio > 125 ppbv) near Washington, D.C., across New Jersey, and in Ohio and western Pennsylvania. The high surface ozone near GSFC on 8 July occurred shortly after MPLNET observations showed the pollutants from the plume mixing to the surface.

[12] On the basis of the data and trajectory calculations presented above we hypothesized that the pollutants from the fires were transported from Canada toward GSFC in an elevated but subsiding plume. A second hypothesis is that this plume was rapidly mixed to the surface over GSFC on 7 July as it was intercepted by the turbulent PBL. To test these hypotheses we simulated the evolution of the smoke plume with a three-dimensional aerosol microphysical and transport model [*Toon et al.*, 1988; *Colarco et al.*, 2002, 2003]. The model dynamics are from the NCEP/NCAR reanalyses, with parameterizations for moist convection, precipitation, and boundary layer mixing from MATCH [*Rasch et al.*, 1997]. Fire locations and timing were prescribed in the model using the fire hot spots identified from GOES-8 imagery. The satellite imagery showed the fires had a distinct diurnal cycle (illustrated schematically in Figure 3). We discuss the magnitude of the smoke emissions used in the model in Appendix A, and our treatment of the aerosol particle size distribution is discussed below and in Appendix A. We note here only that those considerations do not affect the interpretation of the three-dimensional transport pattern of the aerosol.

[13] We find the modeled three-dimensional distribution of smoke, especially the vertical profile at GSFC, to be most sensitive to the height at which we assume emissions from

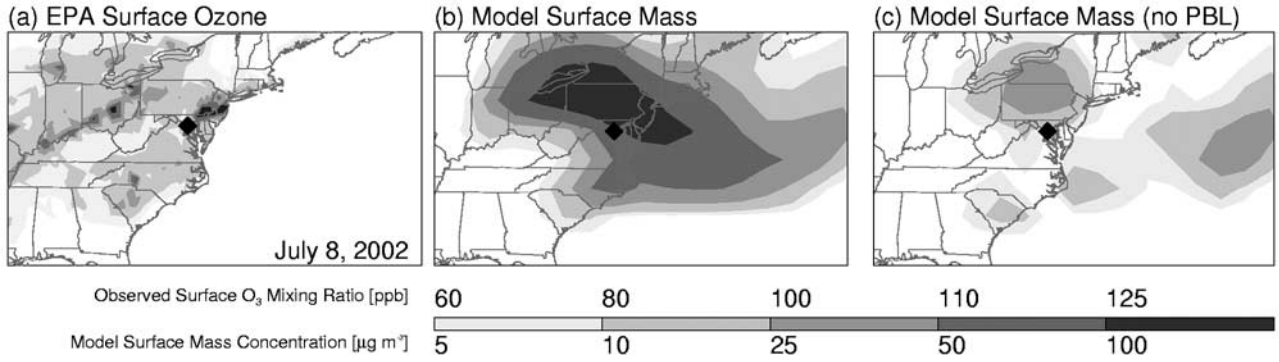

Figure 5. (a) EPA peak 1-hour average surface ozone mixing ratios on 8 July 2002. Also shown are the modeled surface mass concentrations of smoke particles for the high-injection model runs (b) with and (c) without PBL entrainment.

the fires occur. It is common in chemical transport modeling to inject fire emissions over some altitude range rather than right at the surface so that the convection and buoyancy associated with the heat and moisture in the forest fire is somehow accounted for [e.g., *Liousse et al.*, 1996; *Lavoué et al.*, 2000]. Typically emissions are distributed throughout the depth of the PBL, or otherwise at some range of altitudes close to the surface. Low-altitude injections (<3 km) were found to be adequate for some cases previously studied [*Wotawa and Trainer*, 2000; *Forster et al.*, 2001]. This may be typical of most Canadian fire events, but there is ample evidence that in large fire complexes or fires occurring near supercell convection related to midlatitude thunderstorms the emissions can be injected into the upper troposphere and even the lower stratosphere [*Fromm et al.*, 2000; *Fromm and Servanckx*, 2003] where they can be subsequently transported over long distances at very high altitudes [*Siebert et al.*, 2000; H. Jost et al., In situ observations of midlatitude forest fire plumes deep in the stratosphere, submitted to *Geophysical Research. Letters*, 2003].

[14] Using the back trajectories shown in Figure 3 as a guide we add smoke to the model during the active fire times by distributing it uniformly between 2 and 6 km altitude over the fire hot spots. Figure 6a shows the resulting vertical smoke mass distribution from the model over GSFC. The model vertical profile is similar to the MPLNET backscatter observations in Figure 2 except that the model shows a high-altitude smoke plume on 7 July that is not observed with MPLNET (indicated approximately by the dashed box). Possibly this peak is real and is not seen with MPLNET because of the signal attenuation discussed above. Turning sources in the model on and off we determined that this high-altitude plume on 7 July is due to the fires burning on 6 July, whereas the rest of the profile, including the elevated plume remnant on 8 July, can be explained almost entirely by the fires burning on 5 July (consistent with our trajectory analysis). The smoke plumes were continuously and clearly visible in GOES-8 daytime imagery. This imagery suggested that most of the smoke over GSFC during this period is from the fires on 5 July, so it is unlikely the high-altitude plume in the model on 7 July is real. If this interpretation is correct it suggests that the smoke emissions occurred at different altitudes on different days, with the 5 July emissions occurring in the 2–6 km altitude range suggested by the trajectory calculations and later emissions occurring possibly at lower altitudes. Note also in Figure 4 that the modeled vertical profile of aerosol scattering and absorption is similar to what was observed with the AZTEC and MPLNET measurements, although because of the model's relatively coarse vertical resolution we do not adequately resolve the very narrow smoke layer

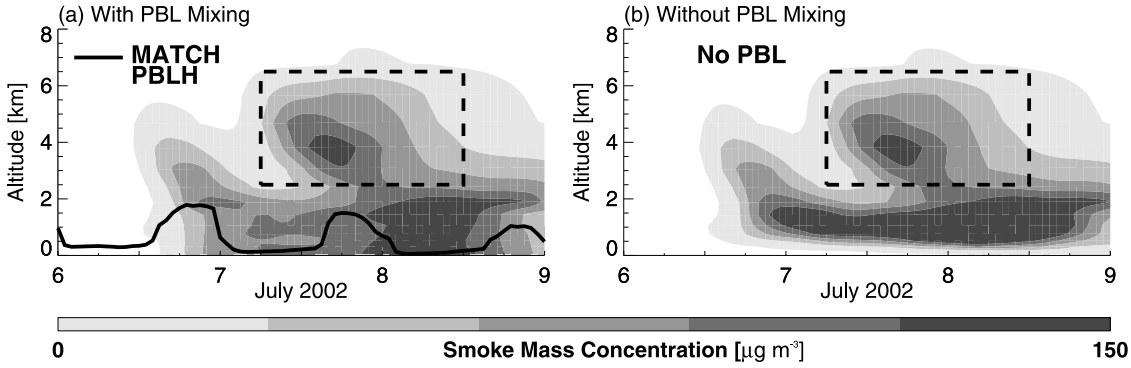

Figure 6. Modeled vertical distribution of smoke aerosol mass at GSFC for the period 6–9 July 2002. (a) Model results with PBL entrainment and (b) model results without PBL entrainment are shown. The solid line is the MATCH PBL height. The dashed box encloses a high-altitude peak in aerosol due to fires burning on 6 July 2002; the remainder of the aerosol is due to the fires burning on 5 July 2002.

observed at precisely the correct altitude (we discuss aerosol optical properties in Section 4).

[15] We tested the model sensitivity to injection altitude by running simulations with injections occurring at other altitudes. In one case we injected all of the smoke at the surface. Because of moist convection over the fire regions on 5 July, a large fraction of this smoke was lifted almost immediately to 2–8 km. In this simulation the vertical profile over GSFC was similar to the case in which all the smoke was injected between 2 and 6 km because in both simulations a great deal of the smoke originated in that altitude range. Because the moist convection was not as strong on 6 July the smoke injected at the surface remained there and the model did not produce a high-altitude plume over GSFC on 7 July. The convective mixing parameterization in the model does not greatly redistribute material already above the surface and below the convective cloud top, so in our initial simulation the plume over the fire region remained relatively intact. Likewise, in another sensitivity test where the smoke was injected between 0.5 and 3 km altitude it descended to the surface rapidly because of subsidence and the vertical profile at GSFC did not agree well with the MPLNET observations. The assumptions about low-altitude injection height used by *Wotawa and Trainer* [2000] and *Forster et al.* [2001] do not appear to apply in this case.

[16] The model largely explains the arrival of an elevated but subsiding plume at GSFC. Subsidence, however, is not sufficient to explain how the material gets to the surface at GSFC. We test the importance of PBL entrainment in the model by turning off the PBL mixing mechanism downwind of the fire regions. For this model run the vertical profile over GSFC looks similar to the baseline simulation shown in Figure 6a except that almost all of the aerosol remains above 500 m (Figure 6b). For the baseline simulation with PBL entrainment, the peak surface mass concentration over GSFC is 140 $\mu g\ m^{-3}$. When PBL entrainment is turned off the peak in the surface mass concentration at GSFC falls to 10 $\mu g\ m^{-3}$. Figures 5b and 5c show the modeled surface mass concentration of the smoke aerosol over the northeastern United States for the simulations both with and without entrainment into the PBL. For the case with PBL entrainment (Figure 5b) the distribution of high surface mass loadings of aerosol is similar to the distribution of high ozone occurrences in the EPA data over Ohio, Pennsylvania, and New Jersey on 8 July (Figure 5a). With PBL entrainment turned off (Figure 5c), however, the distributions look very different. We conclude then that aerosol from the fires was transported mainly in an elevated plume, and that entrainment into the PBL was critical to bringing the aerosol to the surface near GSFC. Other pollutants transported with the aerosol in the plume (e.g., CO, NO, and O_3) would have been transported in a similar fashion.

[17] In summary, the modeled vertical profile at GSFC was similar to the MPLNET observations only when some of the smoke was lifted to 2–6 km over the fire regions on 5 July. Self-lofting because of the heat of the fires offers one explanation of how this may have happened. Alternatively, some combination of heat from the fires and moist convection occurring near the fires offers a plausible mechanism for explaining how the altitude of injection can vary from day to day. The assumptions about fire emission heights used in other studies [*Wotawa and Trainer*, 2000; *Forster et al.*, 2001] do not yield satisfactory results in this simulation, and the fires in this case appear to be more like the convectively influenced cases described by *Fromm et al.* [2000] and *Fromm and Servranckx* [2003]. Finally, the model showed that subsidence alone was not enough to explain how smoke from the fires was transported from an elevated layer to the surface near GSFC. Interception and subsequent entrainment of the elevated aerosol layer by the diurnally varying turbulent PBL provides a mechanism for rapidly mixing the aerosol layer down to the surface.

4. Smoke Plume Optical Properties

[18] Our understanding of smoke optical properties has increased in recent years thanks to field campaigns such as the Smoke, Clouds, and Radiation-Brazil (SCAR-B) experiment [*Kaufman et al.*, 1998] and the Southern Africa Regional Science Initiative (SAFARI 2000) [*Swap et al.*, 2003]. While most such experiments have focused on smoke from tropical fires, there have been relatively few experiments devoted to smoke from boreal forest fires. *Fiebig et al.* [2002, 2003] present data for an aged (6–7 days old) Canadian smoke plume observed over Germany. The spectral AOT from the Aztec, AERONET, and EP-TOMS observations presented here contribute important constraints on optical properties of boreal forest fire smoke that has been transported over somewhat shorter distances and for a shorter period of time.

[19] We focus here on the spectral AOT measurements made by AERONET and onboard the Aztec. These measurements can be used to formulate the Ångström exponent, α:

$$\alpha = -\frac{\ln\left(\tau_1 \Big/ \tau_2\right)}{\ln\left(\lambda_1 \Big/ \lambda_2\right)}, \tag{1}$$

where λ_1 and λ_2 are a pair of measurement wavelengths and $\tau_{\lambda 1}$ and $\tau_{\lambda 2}$ are the AOT values measured at those wavelengths. The Ångström exponent is a standard optical analysis parameter related principally to the aerosol particle size distribution. In general, a small value of α ($\alpha < 1$, relatively little dependence of AOT on wavelength) is associated with large particles while larger values of α are associated with small particles.

[20] The AERONET AOT measurements at GSFC on 7–8 July were among the highest values ever recorded in the entire network [*Eck et al.*, 2003]. The Ångström exponents derived from the AERONET and Aztec measurements near GSFC are small compared to observations made closer to boreal forest fire sources [*O'Neill et al.*, 2002]. These observations are consistent with a smoke plume in which the particles have grown ("aged") considerably during transport. Various mechanisms can explain the smoke particle aging, including hygroscopic water uptake [*Hobbs et al.*, 1997], condensation of volatile organic species [*Reid et al.*, 1998], and coagulation [*Westphal and Toon*, 1991; *Radke et al.*, 1995; *Fiebig et al.*, 2003].

[21] Integrating these aging mechanisms and the observations into our aerosol model is a formidable challenge. At

this point we cannot treat all possible microphysical processes. For example, mixing of the smoke plume with anthropogenic pollutants in the PBL could also alter the optical properties [*Kreidenweis et al.*, 2001]. Since the plume remains above the PBL for most of its transport, however, for simplicity we focus only on coagulation of smoke particles within the plume. We treat the aerosol particle size distribution with a bin (or "sectional") representation, using 16 size bins spaced logarithmically in radius from 0.01 to 1 μm, which makes the treatment of coagulation numerically straightforward [*Toon et al.*, 1988]. Without coagulation, the particle size distribution is essentially unmodified by removal processes. With coagulation the particle size distribution shifts toward larger particles. At the particle sizes and number concentrations typical in our simulation coagulation is important only in about the first two days following emissions (see below). Because the particle sizes remain submicron, coagulation does not affect the vertical distribution of aerosols.

[22] For all simulations we initialize the model with a particle size distribution representative of fresh boreal smoke emissions (see Appendix A). We make no assumptions about the smoke aerosol composition other than its refractive index, for which we use the wavelength-dependent, complex refractive index retrieved from the AERONET almucantar scan of the smoke plume over GSFC made on 8 July 2002 at GSFC (Table 1) [*Dubovik and King*, 2000].

[23] In Figure 7 we compare the modeled particle size distribution over GSFC on 8 July 2002 with the particle size distribution retrieved from AERONET [*Dubovik and King*, 2000]. We recall from Figure 4 that the model had about the right vertical distribution of smoke aerosols on that day. Note that AERONET retrieves a column integrated particle size distribution, so that the retrievals on 8 July include not only the contribution from the smoke aerosol but also any anthropogenic pollutants present. From the AZTEC profiles discussed earlier we know that pollution aerosols are present mainly in lowest 2 km and are optically less important than the smoke aerosol. The AERONET particle size distribution on 8 July has a peak in the volume mode at around 0.2 μm radius, and on the basis of the AZTEC and MPLNET vertical profiles discussed above we expect that the atmospheric column was being optically impacted most by the smoke aerosol overhead on that day. The particle size distribution from the model run with coagulation agrees very well with the AERONET retrieval. Without coagulation, the modeled particle size distribution is shifted toward particles too small to agree with the AERONET retrieval.

[24] Table 2 summarizes the observed and modeled optical properties of the smoke plume near GSFC on 8 July. The EP-TOMS 380 nm AOT is from the closest satellite

Table 1. Wavelength-Dependent Complex Index of Refraction From the AERONET Almucantar at GSFC at 12:38 UTC on 8 July 2002

λ, nm	N_{ref}
440	1.524 – 0.0056*i*
670	1.554 – 0.0043*i*
870	1.573 – 0.0038*i*
1020	1.583 – 0.0037*i*

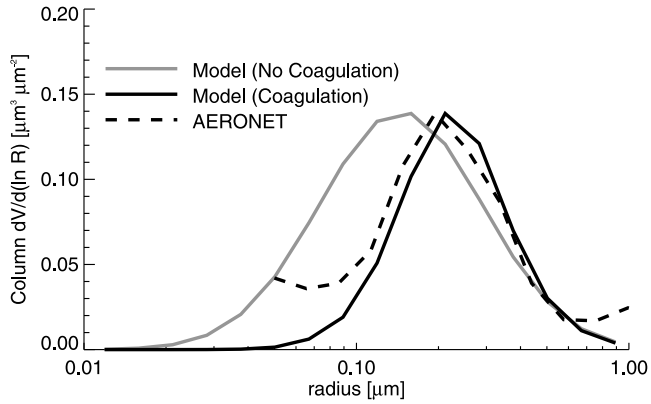

Figure 7. Observed and modeled aerosol particle size distribution at GSFC on 8 July 2002. The size distributions are integrated over the atmospheric column and normalized to the same peak value in the volume. Recall that the model does not contain anthropogenic aerosols in the PBL, which are seen by AERONET if present. Lighter line is the size distribution from the simulation with coagulation turned off. Darker line is from the simulation with coagulation turned on. Dashed line is the AERONET retrieval.

footprint to GSFC, and is 20–30% larger than the AERONET measurements occurring within 30 min of the satellite overpass. This difference is likely related to the large EP-TOMS footprint relative to the essentially point-like AERONET measurement, and is possibly affected by subgridscale cloud contamination. The AERONET measurements at longer wavelengths are comparable to the column AOT measurements from the Aztec profiles of the smoke plume. The model AOT is at the high end of the range of AERONET and Aztec measurements shown, but is slightly smaller than the EP-TOMS retrieval.

[25] The single-scatter albedo from the AERONET retrieval and Aztec measurements indicate a weakly absorbing aerosol. The model single-scatter albedo agrees best with the AERONET measurements, although the AERONET and Aztec values are almost within each other's error bars. The lower single-scatter albedo determined from EP-TOMS is mainly because the optical effective radius of the smoke particle size distribution assumed in the retrieval is too small compared to the AERONET measurements of this plume. Underestimating the particle effective radius makes the aerosol look more absorbing than it actually is, but has only a small effect on the retrieved AOT [*Torres et al.*, 2002]. Note that the model calculated and AERONET retrieved single-scatter albedos are relatively independent of wavelength for the cases discussed here.

[26] Scattering Ångström exponents determined inside the smoke plume from the Aztec nephelometer measurements [*Taubman et al.*, 2004] are recorded for each wavelength pair in Table 2. For the model run with particle coagulation the Ångström exponents calculated at GSFC on 8 July are similar to the values determined from the aircraft measurements. Without coagulation, however, the model's values are much larger than and outside the error bars of the observations. The comparison of the model results with the AERONET scattering Ångström exponent for the 440–670 nm wavelength pair is somewhat ambiguous, probably

Table 2. Aerosol Optical Thickness (τ), Single-Scattering Albedo (ω_0), and Ångström Exponent (α) Values at Selected Wavelengths for the Smoke Aerosol Observed Near GSFC on 8 July[a]

	UTC	τ_{380}	τ_{500}	τ_{550}	τ_{870}	ω_0	$\alpha_{450/550}$	$\alpha_{450/700}$	$\alpha_{550/700}$
EP-TOMS	16:11	2.77				0.89			
AERONET	15:42–16:27	2.09–2.32	1.75–1.96		0.75–0.84	0.97 ± 0.03		1.24[b]	
Aztec	20:00			1.53 ± 0.34		0.93 ± 0.01	0.71 ± 0.10	0.97 ± 0.09	1.18 ± 0.09
Model (coag.)	20:00	2.32	1.91	1.74	0.91	0.98	0.86	1.05	1.20
Model (no coag.)	20:00	1.96	1.39	1.22	0.55	0.98	1.33	1.46	1.57

[a]Shown are (1) the EP-TOMS retrieved AOT and single-scatter albedo (380 nm) for the satellite footprint closest to GSFC, (2) the AERONET AOT (380, 500, and 870 nm) over the 1 hour period enclosing the EP-TOMS overpass, and (3) the Aztec AOT (550 nm), single-scatter albedo (550 nm), and Ångström exponents for the Easton profile. Also shown are the model-computed values at GSFC at the time of the Aztec's Easton profile for runs both with and without coagulation (single-scatter albedo reported at 440 nm). Note that for the AERONET retrievals the single-scatter albedo (440 nm) and Ångström exponent reported are from the almucantar scan at 12:38 UTC since no almucantar scans were performed during the EP-TOMS overpass. The AERONET AOT is slightly smaller at the time the almucantar scan was taken (τ_{380} = 1.75) than during the EP-TOMS overpass.
[b]The AERONET Ångström exponent is actually for the 440–670 nm wavelength pair.

indicating the influence of fine mode particles in the boundary layer on the column integrated properties.

[27] There are uncertainties in comparing the model to these measurements. Because of its coarse spatial resolution it is difficult to justify comparing the model at the scale of a single-grid column to the essentially point-like measurements from the aircraft profiles and the sunphotometer measurements. On the other hand, the spatial extent of the plume is comparable to the model grid size. The net result is that there is not much variability in the modeled particle size distribution and computed Ångström exponents at GSFC or in surrounding grid cells over the period 12:00 UTC 8 July to 00:00 UTC 9 July. In contrast, there is significant variability in the Ångström exponents from the Aztec profiles that sampled the smoke plume (Table 3). There are additional uncertainties associated with the relatively simple treatment of the cycle of smoke emissions (see the Appendix).

[28] Other uncertainties are associated with the choice of refractive index used in calculating the modeled aerosol optical properties. For example, AERONET measurements at the Maryland Science Center in Baltimore, MD (39.27° N, 76.62° W), observed the same smoke plume on 8 July that was seen at GSFC, but because of the spatial and temporal variability of the plume somewhat different refractive indices were retrieved than those shown in Table 1. In Table 3 we summarize the Ångström exponents from the Aztec flights sampling the smoke plume and from the model for various choices of refractive index. The model results shown are all from the simulation in which particles were allowed to coagulate. For most choices of refractive index shown in Table 3 the computed Ångström exponents fit somewhere in the range of values observed by the Aztec. The tendencies are for a decrease in Ångström exponent with an increase in either the real or imaginary component of the refractive index. Although we do not show the variability of Ångström exponents for the model runs without coagulation it is clear that for a given choice of refractive index the Ångström exponents will always be larger in the run without coagulation than in the run with coagulation. For a reasonable range of refractive index, then, the model looks most like the aircraft measurements when coagulation is accounted for. This implies that the smoke particles are larger at GSFC than they were assumed to be at the source region, and that coagulation provides a reasonable explanation for how this growth occurred. In Table 3 we also show the single-scatter albedo from the Aztec measurements and the values calculated in the model for various choices of refractive index. As noted above, the relatively high value of single-scatter albedo in the model tends to agree better with AERONET than with the Aztec measurements. This is true even when the AERONET derived refractive index values are not used, although we see that for somewhat more absorbing aerosols (i.e., the imaginary component of the refractive index is increased) we can obtain better agreement between the model and the

Table 3. Scattering Ångström Exponents and Single-Scattering Albedo (550 nm) of the Smoke Plume Near GSFC on 8 July 2002[a]

Aztec Profile	$\alpha_{450/550}$	$\alpha_{450/700}$	$\alpha_{550/700}$	ω_0	Notes
Luray	0.57 ± 0.18	0.83 ± 0.15	1.04 ± 0.11	0.91 ± 0.02	38.70°N, 78.48°W, 13:00 UTC
Winchester	0.60 ± 0.44	0.85 ± 0.32	1.05 ± 0.22	0.94 ± 0.01	39.15°N, 78.15°W, 14:00 UTC
Easton	0.71 ± 0.10	0.97 ± 0.09	1.18 ± 0.09	0.93 ± 0.01	38.80°N, 76.06°W, 20:00 UTC
Harford	0.87 ± 0.10	1.09 ± 0.09	1.26 ± 0.09	0.93 ± 0.01	39.56°N, 76.18°W, 19:00 UTC
Model Profile					
Case 1	0.86	1.05	1.20	0.98	N_{ref} from AERONET at GSFC (Table 1).
Case 2	0.98	1.20	1.38	0.97	N_{ref} from AERONET at Maryland Science Center [*Eck et al.*, 2003].
Case 3	0.94	1.18	1.37	0.95	λ-independent $N_{ref} = 1.55 - 0.01i$ [*Westphal and Toon*, 1991].
Case 4	1.10	1.31	1.48	0.95	λ-independent $N_{ref} = 1.50 - 0.01i$.
Case 5	0.80	1.06	1.27	0.95	λ-independent $N_{ref} = 1.60 - 0.01i$.
Case 6	0.96	1.19	1.39	0.97	λ-independent $N_{ref} = 1.55 - 0.005i$.
Case 7	0.93	1.16	1.36	0.93	λ-independent $N_{ref} = 1.55 - 0.015i$ [*Torres et al.*, 2002].
Case 8	0.88	1.11	1.31	0.85	λ-independent $N_{ref} = 1.55 - 0.035i$ [*Torres et al.*, 2002].

[a]Shown are the four Aztec measurements at the altitude of the smoke layer. Also shown are the modeled Ångström exponents and single-scatter albedo at GSFC for several choices of complex index of refraction (references are indicated for published values).

Aztec measurements and still maintaining agreement in the Ångström exponents. It remains an open question whether the wavelength-dependent choice of refractive index (from the AERONET inversion) is a better choice of refractive index than the wavelength-dependent values used in the sensitivity studies.

[29] There are additional uncertainties in our results which can be related to how coagulation is treated. In particular, we consider the study of an aged forest fire plume discussed by *Fiebig et al.* [2003]. They point out that the rate of coagulation in the aging smoke plume is strongly controlled by the rate at which the air is diluted; that is, as turbulent eddies mix relatively clean ambient air into the plume the rate at which smoke particles coagulate should decrease. We do not explicitly account for plume dilution in our model, but since our model is Eulerian and of relatively coarse spatial resolution there is significant numerical diffusion associated with our advection algorithm which effectively dilutes the plume. Furthermore, air entrained in the boundary layer undergoes turbulent mixing as parameterized by our PBL scheme. In our sensitivity tests with no coagulation the peak number concentration occurs over the (essentially point-like) sources and is reduced by about 2/3 for the portion of the plume advected over GSFC two days later. This can be taken as a rough measure of the plume dilution during transport. In the simulations which include coagulation the number concentration is reduced a further 2/3 at GSFC relative to the peak number concentration over the source region. That is, the number concentration at GSFC two days after the fires is about 10% the peak number concentration over the source region during the fires for the simulations which include coagulation. Because of the plume dispersion coagulation is relatively unimportant after about two days.

[30] These results cannot be easily compared with the analysis *Fiebig et al.* [2003] did for the forest fire plume transported from Canada to western Europe. For one thing, they made different assumptions about the initial particle size distribution than we did. Additionally, their detailed results are only reported for a plume aged six days, while our own results pertain to a plume aged only about two days. Our results suggest that the plume has diluted significantly in transit, but this does not preclude *Fiebig et al.*'s [2003] conclusion that plume dilution may be significantly inhibited by radiative-convective mixing in the absorbing aerosol layer. Our model was tuned to give the correct optical depth at GSFC; in a less diffusive model we would have chosen different initial conditions and our results would have been different. Treatment of the plume in a Lagrangian framework is beyond the scope of this study, but if coupled with observations both nearer and farther from the fire such a study would help to better constrain the importance of coagulation. For now, in the context of this simulation, we conclude it is a plausible mechanism to explain the observed optical properties.

[31] In summary, the modeled particle size distribution was shown to be similar to the AERONET retrieval for simulations when particle growth by coagulation was accounted for. Simulated values of single-scattering albedo and wavelength-dependent Ångström exponents are similar to the AZTEC observations for the cases with coagulation. There are uncertainties associated with our choice of the refractive index, which causes small variations in the wavelength-dependent AOT calculated that can lead to large variations in the Ångström exponent. The Ångström exponent is a primary indicator of particle size, however, so despite our uncertainties in the refractive index there is always a clear difference in the Ångström exponents when the model runs with and without coagulation are compared. The model results are much more coherent with the observations for the runs with coagulation than they are for runs which neglect this process. This leads us to conclude that coagulation can be important to modifying the initial aerosol particle size distribution and can explain at least some of the observed spectral dependence in the AOT far downwind. This has implications to radiative forcing calculations as well as retrievals of aerosol properties made from satellite observations. Neglecting the aging of aerosol particles in smoke plumes and instead relying on particle size distributions measured near the smoke emission point for these calculations will yield the wrong spectral dependence in the optical properties. These conclusions about the importance of coagulation are consistent with other studies of aging forest fire plumes [e.g., *Westphal and Toon*, 1991; *Fiebig et al.*, 2003], but there are considerable uncertainties associated with how this process should be treated in our model.

5. Conclusions

[32] Our analysis of the transport of a Canadian forest fire plume over the eastern United States during July 2002 demonstrates that an important mechanism for transporting pollutants from elevated layers to the surface is by entrainment into the PBL of a gradually subsiding plume. An aerosol microphysics and transport model driven by assimilated meteorology confirms this mechanism. This model also tested various assumptions about the initial injection altitude of the plume from the fires. The modeled vertical profile at GSFC was similar to the MPLNET observations provided the majority of the smoke was initially injected into a 2–6 km altitude layer, as suggested by our trajectory calculations. Moist convection over the fire regions can explain how this elevated layer developed. Our simulation yielded spectral AOT values similar to those observed with the aircraft flights and sunphotometer measurements provided we accounted for modification of the smoke particle size distribution by coagulation. The largest uncertainties in our simulations are in our specification of the aerosol sources, including the emission magnitude and the altitude of emission injection, in the refractive index assumed in the calculation of aerosol optical properties, and in how coagulation and plume dilution are treated in the model.

[33] The aerosol lifting and deposition mechanisms discussed here have important implications for the long-range transport of smoke aerosols from boreal forest fires and their effects at the surface through subsequent coupling to the PBL downstream. Accounting for the modification of the smoke aerosol particle size distribution due to coagulation and other modification processes is also important for correctly determining the direct radiative effect of the aerosol, as well as for quantitative retrievals of aerosol properties from remote sensing measurements. Future analyses will incorporate additional aerosol growth mechanisms

into our microphysical model, as well as producing simulations with a higher vertical resolution to improve the vertical placement of elevated plumes. Finally, it is anticipated that the satellite data used to detect fire locations can eventually provide some estimates of fire intensity, which in turn will help constrain the altitude at which smoke plume emissions occur.

Appendix A: Model Description

[34] Our aerosol model [*Colarco et al.*, 2002, 2003] couples dynamical fields from the NCEP/NCAR reanalyses [*Kalnay et al.*, 1996] and the NCAR Model for Atmospheric Transport and Chemistry (MATCH) [*Rasch et al.*, 1997] to the University of Colorado/NASA Ames Community Aerosol and Radiation Model for Atmospheres (CARMA) [*Toon et al.*, 1988]. CARMA is a bin-resolving microphysical model which solves the aerosol continuity equation for source, transport, removal, and transformational processes (e.g., coagulation). The NCEP/NCAR reanalyses and MATCH provide wind, temperature, and pressure fields, as well as convective mass fluxes, precipitation rates, and eddy diffusion coefficients for mixing in the planetary boundary layer. These fields are archived globally every hour of model time at the spatial resolution of the NCEP/NCAR reanalyses (approximately $1.875° \times 1.875°$ in the horizontal and 28 vertical sigma levels from the surface to about 28 km). CARMA is run on a limited domain encompassing most of North America and the North Atlantic Ocean with the same grid spacing. The model is run from 5 to 11 July with an 1800 second time step and we linearly interpolate the input dynamical fields to the current time step.

[35] The timing and locations of fire hot spots are determined from the 4 μm and 11 μm GOES-8 channels [*Prins and Menzel*, 1992]. The locations of fire hot spots on 5 July 2002 are shown in Figure 1b, and the active fire times are indicated by the grey bars in Figure 3. We assume that the fires are emitting at a constant rate while the fires are active. We assume a flux of 5×10^{-8} kg m^{-2} s^{-1} per hot spot, which yields total emissions of about 1.5 Tg. The injection altitude of the smoke particles is as described in the text.

[36] We do not have a data set to quantify the actual smoke emissions. A rough estimate was obtained by assuming typical land surface characteristics and assuming 250,000 ha of land burned, where we assume average biofuel loadings of 27 Mg ha^{-1} of aboveground carbon material (consumed with 22% efficiency) and 134 Mg ha^{-1} of ground level carbon material (consumed with 6% efficiency) (using the "Boreal East" statistics by *Kasischke et al.* [2000]Table 2). Assuming the carbon content is 45% of the total dry matter mass and applying a typical emission factor of 0.013 g PM2.5 per 1 g dry matter burned [*Andreae and Merlet*, 2001] we estimate total PM2.5 emissions from the fires to be about 0.10 Tg, which is about a factor of 10 smaller than the emissions used in the model. The emissions used in the model were tuned to give reasonable agreement between the model and observed aerosol optical properties at GSFC. Reducing the model emissions to 0.10 Tg results in a dramatic decrease in the AOT at GSFC so that the model greatly underestimates the observed AOT. We point out that there is considerable uncertainty in this emission estimate because we are applying average land spatial characteristics and assuming a smoke emission factor which may not be representative of the actual fires. Alternatively, because of numerical diffusion and the model's coarse spatial resolution we may require unrealistically large total emissions in order to get 200 km × 200 km grid cells to represent aerosol distributions which might be present on much smaller scales. Higher spatial resolution simulations will answer this question, but for now we are satisfied to get reasonably AOT agreement between the model and the observations.

[37] The injected smoke particles are distributed across 16 size bins spaced logarithmically in radius between 0.01 and 1 μm. There are observations of coarse mode particles with radius >1 μm in boreal forest fire plumes [*Radke et al.*, 1991]. These particles are usually ash, partially burned foliage, and lofted soil particles that make up a small fraction of the total particulate mass, have large fall speeds, and are less optically efficient than the fine mode particles. We neglect these large particles in this study of long-range transport of smoke, although they may be important to the properties of the smoke plume near the sources. We assume the smoke particles have a lognormal size distribution with a volume mode radius of 0.145 μm and a standard deviation of 2.00 [*Westphal and Toon*, 1991]. This initial particle size distribution is similar to a recent climatology of South American and African biomass burning aerosols determined from AERONET observations near major source regions [*Dubovik et al.*, 2002]. The density of the particles is assumed to be 1.35 g cm^{-3} [*Reid et al.*, 1998]. Sedimentation, dry deposition, and precipitation scavenging rates are determined for each size bin [*Colarco et al.*, 2003]. For some of our simulations we allow coagulation to modify the particle size distribution, which increases the mean radius of the particle size distribution at a rate approximately proportional to the air temperature, the square of the particle number concentration, and the inverse of the particle radius [*Prupacher and Klett*, 1997]. Our algorithm [*Toon et al.*, 1988] preserves the total aerosol volume but decreases the number concentration of particles as small particles stick together and grow larger.

[38] We calculate the smoke optical properties in the model assuming a wavelength-dependent refractive index based on AERONET almucantar retrievals of the smoke plume over GSFC [*Holben et al.*, 1998; *Dubovik and King*, 2000]. AERONET inverts aerosol optical properties by fitting radiance measurements over a wide angular and spectral range (the almucantar scan) to a precomputed look-up table of radiances. The retrieval provides the column integrated aerosol particle size distribution, and the complex index of refraction and single-scatter albedo at four reference wavelengths (440, 670, 870, and 1020 nm). Because of restrictions on the inversion the retrievals are only valid for almucantar scans taken at high solar zenith angle ($\geq 45°$) and high AOT ($\tau_{440} \geq 0.4$). Additional screening criteria may further restrict the availability of retrievals (see http://aeronet.gsfc.nasa.gov/). For this study we use a complex index of refraction from the AERONET almucantar scan taken at 12:38 UTC at GSFC on 8 July 2002 (Table 1). Refractive indices at other than the reference wavelengths are computed by a least squares

second-order polynomial fit to the retrieved values. These refractive indices are representative of the atmospheric column over GSFC at the time the scan was taken, although because of the high AOT of the smoke plume (Table 2) we expect that contributions from other aerosols present (e.g., anthropogenic pollutants) will have only a minor effect on the column integrated value. Optical properties of the aerosols in the model are calculated from the simulated particle size distributions with a Mie scattering code [*Wiscombe*, 1980].

[39] **Acknowledgments.** This research was partially funded by the NASA Interdisciplinary Science program. BGD and LTM acknowledge support from Maryland Department of Environment and Mid-Atlantic and Northeast Visibility Union. The Micro-Pulse Lidar NETwork (MPLNET) is funded by the NASA Earth Observing System. B. N. Holben provided AERONET data. T. F. Eck and B. F. Taubman provided valuable comments to this manuscript. The SeaWiFS imagery is courtesy of SeaWiFS Project, NASA Goddard Space Flight Center, and ORBIMAGE.

References

Andreae, M. O., and P. Merlet (2001), Emission of trace gases and aerosols from biomass burning, *Global Biogeochem. Cycles*, *15*, 955–966.

Campbell, J. R., D. L. Hlavka, E. J. Welton, C. J. Flynn, D. D. Turner, J. D. Spinhirne, V. S. Scott, and I. H. Hwang (2002), Full-time, eye-safe cloud and aerosol lidar observation at atmospheric radiation measurement program sites: Instruments and data processing, *J. Atmos. Oceanic Technol.*, *19*, 431–442.

Colarco, P. R., O. B. Toon, O. Torres, and P. J. Rasch (2002), Determining the UV imaginary index of refraction of Saharan dust particles from Total Ozone Mapping Spectrometer data using a three-dimensional model of dust transport, *J. Geophys. Res.*, *107*(D16), 4289, doi:10.1029/2001JD000903.

Colarco, P. R., O. B. Toon, and B. N. Holben (2003), Saharan dust transport to the Caribbean during PRIDE: 1. Influence of dust sources and removal mechanisms on the timing and magnitude of downwind aerosol optical depth events from simulations of in situ and remote sensing observations, *J. Geophys. Res.*, *108*(D19), doi:10.1029/2002JD002658.

Dubovik, O., and M. D. King (2000), A flexible inversion algorithm for retrieval of aerosol optical properties from Sun and sky radiance measurements, *J. Geophys. Res.*, *105*, 20,673–20,696.

Dubovik, O., B. Holben, T. F. Eck, A. Smirnov, Y. J. Kaufman, M. D. King, D. Tanré, and I. Slutsker (2002), Variability of absorption and optical properties of key aerosol types observed in worldwide locations, *J. Atmos. Sci.*, *59*, 590–608.

Eck, T. F., B. N. Holben, J. S. Reid, N. T. O'Neill, J. S. Schafer, O. Dubovik, A. Smirnov, M. A. Yamasoe, and P. Artaxo (2003), High aerosol optical depth biomass burning events: A comparison of optical properties for different source regions, *Geophys. Res. Lett.*, *30*(20), 2035, doi:10.1029/2003GL017861.

Fiebig, M., et al. (2002), Optical closure for an aerosol column: Method, accuracy, and inferable properties applied to a biomass-burning aerosol and its radiative forcing, *J. Geophys. Res.*, *107*(D21), 8130, doi:10.1029/2000JD000192.

Fiebig, M., A. Stohl, M. Wendisch, S. Eckhardt, and A. Petzold (2003), Dependence of solar radiative forcing of forest fire aerosol on ageing and state of mixture, *Atmos. Chem. Phys.*, *3*, 881–891.

Forster, C., et al. (2001), Transport of boreal forest fire emissions from Canada to Europe, *J. Geophys. Res.*, *106*, 2887–2906.

Fromm, M. D., and R. Servanckx (2003), Transpport of forest fire smoke above the tropopause by supercell convection, *Geophys. Res. Lett.*, *30*(10), 1542, doi:10.1029/2002GL016820.

Fromm, M., J. Alfred, K. Hoppel, J. Hornstein, R. Bevilacqua, E. Shettle, R. Servanckx, Z. Q. Li, and B. Stocks (2000), Observations of boreal forest fire smoke in the stratosphere by POAM III, SAGE II, and lidar in 1998, *Geophys. Res. Lett.*, *27*, 1407–1410.

Goode, J. G., R. J. Yokelson, D. E. Ward, R. A. Susott, R. E. Babbitt, M. A. Davies, and W. M. Hao (2000), Measurements of excess O_3, CO_2, CO, CH_4, C_2H_4, C_2H_2, HCN, NO, NH_3, HCOOH, CH_3COOH, HCHO, and CH_3OH in 1997 Alaskan biomass burning plumes by airborne Fourier transform infrared spectroscopy (AFTIR), *J. Geophys. Res.*, *105*, 2147–2166.

Hobbs, P. V., J. S. Reid, R. A. Kotchenruther, R. J. Ferek, and R. Weiss (1997), Direct radiative forcing by smoke from biomass burning, *Science*, *275*, 1776–1778.

Holben, B. N., et al. (1998), AERONET-A federated instrument network and data archive for aerosol characterization, *Remote Sens. Environ.*, *66*, 1–16.

Kalnay, E., et al. (1996), The NCEP/NCAR 40-year reanalysis project, *Bull. Am. Meteorol. Soc.*, *77*, 437–471.

Kasischke, E. S., B. J. Stocks, K. O'Neill, N. H. F. French, and L. L. Bourgeau-Chavez (2000), Direct effects of fire on the boreal forest carbon budget, in *Biomass Burning and Its Inter-relationships With the Climate System*, edited by J. L. Innes, M. Beniston, and M. M. Verstraete, pp. 51–68, Kluwer Acad, Norwell, Mass.

Kaufman, Y. J., et al. (1998), Smoke, Clouds, and Radiation-Brazil (SCAR-B) experiment, *J. Geophys. Res.*, *103*, 31,783–31,808.

Kreidenweis, S. M., L. A. Remer, R. Bruintjes, and O. Dubovik (2001), Smoke aerosol from biomass burning in Mexico: Hygroscopic smoke optical model, *J. Geophys. Res.*, *106*, 4831–4844.

Lavoué, D., C. Liousse, H. Cachier, B. J. Stocks, and J. G. Goldammer (2000), Modeling of carbonaceous particles emitted by boreal and temperate wildfires at northern latitudes, *J. Geophys. Res.*, *105*, 26,871–26,890.

Lelieveld, J., et al. (2002), Global air pollution crossroads over the Mediterranean, *Science*, *298*, 794–799.

Liousse, C., J. E. Penner, C. Chuang, J. J. Walton, H. Eddleman, and H. Cachier (1996), A global three-dimensional model study of carbonaceous aerosols, *J. Geophys. Res.*, *101*, 19,411–19,432.

O'Neill, N. T., T. F. Eck, B. N. Holben, A. Smirnov, A. Royer, and Z. Li (2002), Optical properties of boreal forest fire smoke derived from Sun photometry, *J. Geophys. Res.*, *107*(D11), 4125, doi:10.1029/2001JD000877.

Prins, E. M., and W. P. Menzel (1992), Geostationary satellite detection of biomass burning in South-America, *Int. J. Remote Sens.*, *13*, 2783–2799.

Prospero, J. M., I. Olmez, and M. Ames (2001), Al and Fe in PM 2.5 and PM 10 suspended particles in south-central Florida: The impact of the long range transport of African mineral dust, *Water Air Soil Pollut.*, *125*, 291–317.

Prupacher, H. R., and J. D. Klett (1997), *Microphysics of Clouds and Precipitation*, Kluwer Acad., Norwell, Mass.

Radke, L. F., D. A. Hegg, P. V. Hobbs, J. D. Nance, J. H. Lyons, K. K. Laursen, R. E. Weiss, P. J. Riggan, and D. E. Ward (1991), Particulate and trace gas emissions from large biomass fires in North America, in *Global Biomass Burning*, edited by J. S. Levine, pp. 209–224, MIT Press, Cambridge, Mass.

Radke, L. F., A. S. Hegg, P. V. Hobbs, and J. E. Penner (1995), Effects of aging on the smoke from a large forest-fire, *Atmos. Res.*, *38*, 315–332.

Rasch, P. J., N. M. Mahowald, and B. E. Eaton (1997), Representations of transport, convection, and the hydrologic cycle in chemical transport models: Implications for the modeling of short-lived and soluble species, *J. Geophys. Res.*, *102*, 28,127–28,138.

Reid, J. S., P. V. Hobbs, R. J. Ferek, D. R. Blake, J. V. Martins, M. R. Dunlap, and C. Liousse (1998), Physical, chemical, and optical properties of regional hazes dominated by smoke in Brazil, *J. Geophys. Res.*, *103*, 32,059–32,080.

Schoeberl, M. R., and L. C. Sparling (1995), Trajectory modeling, in *Diagnostic Tools in Atmospheric Physics: Enrico Fermi Course CXVI*, edited by G. Fiocco and G. Visconti, pp. 289–305, North-Holland, New York.

Siebert, J., C. Timmis, G. Vaughan, and K. H. Fricke (2000), A strange cloud in the Artic summer stratosphere 1998 above Esrange (68°N), Sweden, *Ann. Geophys.*, *18*, 505–509.

Spichtinger, N., M. Wenig, P. James, T. Wagner, U. Platt, and A. Stohl (2001), Satellite detection of a continental-scale plume of nitrogen oxides from boreal forest fires, *Geophys. Res. Lett.*, *28*, 4579–4582.

Swap, R. J., H. J. Annegarn, J. T. Suttles, M. D. King, S. Platnick, J. L. Privette, and R. J. Scholes (2003), Africa burning: A thematic analysis of the Southern African Regional Science Initiative (SAFARI 2000), *J. Geophys. Res.*, *108*(D13), 8465, doi:10.1029/2003JD003747.

Taubman, B. F., L. T. Marufu, B. L. Vant-Hull, C. A. Piety, B. G. Doddridge, R. R. Dickerson, and Z. Li (2004), Smoke over haze: Aircraft observations of chemical and optical properties and the effects on heating rates and stability, *J. Geophys. Res.*, *109*, D02206, doi:10.1029/2003JD003898.

Toon, O. B., R. P. Turco, D. Westphal, R. Malone, and M. S. Liu (1988), A multidimensional model for aerosols—Description of computational analogs, *J. Atmos. Sci.*, *45*, 2123–2143.

Torres, O., P. K. Bhartia, J. R. Herman, A. Sinyuk, P. Ginoux, and B. Holben (2002), A long-term record of aerosol optical depth from TOMS observations and comparison to AERONET measurements, *J. Atmos. Sci.*, *59*, 398–413.

Welton, E. J., J. R. Campbell, J. D. Spinhirne, and V. S. Scott (2001), Global monitoring of clouds and aerosols using a network of micro-pulse lidar systems, in *Lidar Remote Sensing for Industry and Environmental Monitoring*, edited by U. N. Singh, T. Itabe, and N. Sugimoto, *Proceedings SPIE Int. Soc. Opt. Eng.*, *4153*, 151–158.

Westphal, D. L., and O. B. Toon (1991), Simulations of microphysical, radiative, and dynamic processes in a continental-scale forest-fire smoke plume, *J. Geophys. Res.*, *96*, 2379–2400.

Wiscombe, W. J. (1980), Improved Mie scattering algorithms, *Appl. Opt.*, *19*, 1505–1509.

Wotawa, G., and M. Trainer (2000), The influence of Canadian forest fires on pollutant concentrations in the United States, *Science*, *288*, 324–328.

P. R. Colarco, M. R. Schoeberl, and O. Torres, NASA Goddard Space Flight Center, Code 916, Greenbelt, MD 20771, USA. (colarco@essic.umd.edu)

B. G. Doddridge and L. T. Marufu, Department of Meteorology, University of Maryland, College Park, MD 20742, USA.

E. J. Welton, NASA Goddard Space Flight Center, Code 912, Greenbelt, MD 20771, USA.